JOURNAL OF APPLIED ELECTROCHEMISTRY 19 (1989) 845–855

Laminar radial flow electrochemical reactors. II. Convective diffusion of inert tracer

F. B. THOMAS

Hycal Energy Research Laboratories Ltd, 1338 A, 36th Ave. N.E., Calgary, Alberta, Canada T2E 6T6

P. A. RAMACHANDRAN, M. P. DUDUKOVIC

Chemical Reaction Engineering Laboratory, Dept. of Chemical Engineering, Washington University, St. Louis, MO 63130, USA

R. E. W. JANSSON

Monsanto Corporation, 800 North Lindbergh Blvd, St. Louis, MO 63137, USA

Received 24 February 1988; revised 16 August 1988

Mixing is investigated in three laminar radial flow cells (capillary gap cell (stationary discs), pump cell (one disc spinning) and the rotating electrolyser (co-rotating discs)) using numerical and semi-analytical methods for inert tracer transport. Results are compared to existing data. Mixing in the three cells is modelled using finite element techniques applied to convection-dominated inert tracer transport. For the capillary gap cell modes of tracer tagging and detection are commented on with respect to which type provides the correct representation of the residence time distribution. The extent of cross-gap communication, from anode to cathode, is quantified and compared to that observed in the other radial cell designs. Two semi-analytical solutions (convection only, Taylor diffusion) are derived for inert tracer transport in this configuration and are compared to the detailed numerical results. Convection only is relevant for t_d/t_c ratios of greater than 100 and the Taylor diffusion model applies for t_d/t_c ratios of about 0.10 and only beyond a critical radius defined herein. Pump cell (PC) mixing is modelled using finite element techniques for the tracer, the velocity field being provided by a semi-analytical solution. Mixing is quantified in this cell and cross-gap communication evaluated. The large axial velocities provide for significant cross-gap mixing. The rotating electrolyser is modelled and the efficiency of separation of catholyte/anolyte streams is observed to be determined by Taylor number (Taylor number (α) – ratio of half-gap width divided by theoretical boundary layer thickness). The superiority of separation in this cell is quantified by definition of the zeroth wall moment and comparison with the other two radial cells. For the example modelled, cross-gap communication was less than half that of the other cells.

Nomenclature

a	gap width (m)
A	half interelectrode gap width (m)
C	dimensionless concentration
D	diffusion coefficient ($m^2\ s^{-1}$)
K	radial Taylor diffusion coefficient (Equation 39)
M_0	normalized zeroth moment (Equation 6)
Pe	Peclet number ($v_c a/D$)
Q	volumetric flow rate ($m^3\ s^{-1}$)
r	dimensionless radius, dimensionless square radius in moving coordinates
R	radius (m)
Re	Reynolds number ($v_c a/\nu$)
Re_θ	rotational Reynolds number ($\omega R_0^2/\nu$)
t	time (s)
τ	dimensionless time (Equation 3), also residence time
v_r	dimensionless radial velocity
v_z	dimensionless axial velocity
V	volume (m^3) and velocity ($m\ s^{-1}$)
z	dimensionless axial distance

Greek and other symbols

α	Taylor number ($(a^2\omega)/4\nu)^{1/2}$)
ε	ratio of characteristic lengths (a/R_0)
ξ	transformed variable for Taylor analysis (Equation 23)
π	constant
ν	kinematic viscosity ($m^2\ s^{-1}$)
ω	angular velocity ($rad\ s^{-1}$)
∞	reference value

Subscripts

CMavg	cup-mix average
RMAX	radial maximum
in	inlet
Ravg-R	average radial velocity at R

0021-891X/89 $03.00 + .12 © 1989 Chapman and Hall Ltd.

1. Introduction

The majority of work done in electroorganic synthesis research has been experimental. To begin to comprehend the factors which contribute to efficient cell design and operation, knowledge of electrochemical cells' mixing environment has been recognized as being of primary importance. This is particularly true of systems involving competing homogeneous reaction steps such as the methoxylation of furan or the electrochemical production of propylene oxide.

This paper discusses mixing effects in the three radial flow cells (the capillary gap cell (stationary discs), the pump cell (one disc spinning) and the rotating electrolyser (co-rotational discs)). Figure 1 presents the geometry of these reactors. In the first section, a brief summary of conventional mixing models is included after which a more rigorous model of inert tracer transport is described. Results are presented for the three cells based on this detailed model. Comparisons are also made with existing experimental data. Two simplified approaches are then applied to the CG cell (Taylor diffusivity analysis and pure convection) and comparisons made to the numerical solution.

2. Mixing models

The axial dispersion model (ADM) is the simplest mathematical description of a flow system where both convection and diffusion effects are important. For a system without homogeneous reaction, the ADM usually assumes the form of

$$\frac{\partial C}{\partial t} = D\frac{\partial^2 C}{\partial Z^2} - V\frac{\partial C}{\partial Z} \tag{1}$$

By comparison with the complete convection–diffusion equation (in cylindrical coordinates and where azimuthal symmetry has been assumed)

$$\frac{\partial C}{\partial t} = D\left(\frac{\partial^2 C}{\partial R^2} + \frac{1}{R}\frac{\partial C}{\partial R} + \frac{\partial^2 C}{\partial Z^2}\right) - \left(v_r\frac{\partial C}{\partial R} + v_z\frac{\partial C}{\partial Z}\right) \tag{2}$$

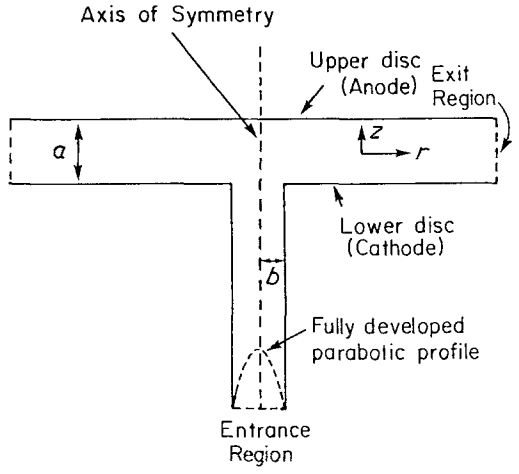

Fig. 1. Radial cell geometry.

one can see that the ADM is strictly applicable for those systems where radial concentration gradients are zero and where v_z equals a constant V; that is, plug flow operation with diffusion effects in the direction parallel to the mean fluid flow. Considerable success has been obtained using the ADM for systems where the influence of the velocity profile is grouped in with the diffusion coefficient. Wen and Fan [1] report the broad range of applicability of the ADM when the dispersion coefficient is defined as: $K = D + V^2R^2/(48D)$.

Fahidy [2] discussed the application of the ADM to electrochemical reactors where all deviations from plug flow behaviour are lumped into the dispersion coefficient. Fleischmann and Jansson [3] applied the ADM methodology to the radial flow geometry. Therein the effects of diffusion, parabolic profile and fluid deceleration were all subsumed under the dispersion coefficient. Their model compared poorly with experiment. Fleischmann and Jansson recognized this deviation as associated with the tracers being generated and detected at the electrodes. The tracer responses would represent a much different residence time distribution than the fluid bulk would possess. Fleischmann *et al.* [4] reported a high degree of segregation (the normalized first moments of the experimental tracer responses were as much as two orders of magnitude greater than those of the model).

Jansson and Marshall [5, 6] successfully applied two empirical models to parallel plate reactors. Despite the success of these simplified models in matching experimental data, their use will be limited for systems involving complex homogeneous reaction paths and high Damkohler numbers. In these cases, one must be able to account for the important phenomena in a more complete and fundamental manner.

Since little has been done to describe mixing in radial flow cells, a mathematical model was developed to predict inert tracer transport within the capillary gap cell, the pump cell and the rotating electrolyser. Comparison can then be made to some limiting cases and possible areas of application deduced.

3. Detailed numerical model

This section describes the development of a detailed mathematical model which quantifies mixing effects in the three laminar radial flow reactors.

3.1. *Problem formulation*

The rotating electrolyser may exhibit a radial velport had negligible effect on the flow field. Since the Peclet number (Pe) is almost always large ($\geqslant 100$), the tracer should have little impact on the velocity profiles. The second assumption is that the diffusion coefficient is a constant. Deviations from this should be small for isothermal systems.

With these assumptions, the velocity profiles (detailed elsewhere [7, 19]) were substituted into the convective

diffusion Equation 3 (or in dimensionless form)

$$\frac{\partial C}{\partial \tau} = \left(\varepsilon^2 \frac{\partial^2 C}{\partial r^2} + \frac{\varepsilon^2 \partial C}{r \partial r} + \frac{\partial^2 C}{\partial z^2}\right) - Pe\left(\varepsilon v_r \frac{\partial C}{\partial r} + v_z \frac{\partial C}{\partial z}\right) \quad (3)$$

where the dimensionless variables defined are

$$\tau = \frac{Dt}{a^2}; C = \frac{C}{C_\infty}; r = \frac{R}{R_0}; z = \frac{Z}{a}$$

$$v_r = \frac{v_r}{v_c}; v_z = \frac{v_z}{v_c}; \varepsilon = \frac{a}{R_0}; Pe = \frac{v_c a}{D}$$

The REL characteristic velocity is defined as the maximum velocity at the inert radius of the pipe (R_{in}). For the other two cells the characteristic velocity used is $v_c = 6Q/(2\pi R_{in} a)$. The boundary conditions then complete the formulation. For the case of inert tracer, the disc surfaces are unreactive and therefore $\partial C/\partial z = 0$. At the inlet to the reactor, the boundary conditions differ according to whether the tracer is bulk or wall generated and whether reverse flows are present. These conditions will now be described according to cell type and inlet–outlet boundary.

At the inlet boundary of the capillary gap cell the boundary conditions are of the essential type – where the value of the concentration is specified (1.0 for this dimensionless form). For wall-generated tracer, an initial point source is present and then removed. This point source is located at a certain radius further out than the cell inlet however, so that 'pure solvent' can be specified at the inlet. Figure 2 illustrates this boundary condition. The distance d_1 was determined by increasing the distance between reactor inlet and the point source until radial back diffusion did not alter the inlet concentrations.

The exit end condition is the standard Danckwert's type $\partial C/\partial r = 0$. In addition the R_0 was specified very large ($\varepsilon = 333$), 3.5 times larger than where the last experimental tracer was detected in the work of Fleischmann *et al.* [4]. Thus negligible error would result from the exit-end boundary conditions.

The pump cell was more involved due to the reverse radial flows. Since considerable reverse radial flows are even possible at the inlet, the simulation had to begin from a smaller radius than where the bulk tracer was injected. This would correspond to the gauze-type tracer injection as described by Jansson [6]. The innermost radius was assigned the $\partial C/\partial r = 0$ condition. For wall tracer the same method was used as for the capillary gap cell.

At the exit end the conditions imposed were $\partial C/\partial r = 0$ across the gap where v_r was positive and C was specified as zero over the region of radial inflow. This would simulate the case where the cell empties into a comparatively very large CSTR, where the concentration in the CSTR always remains negligible. Where tracer accumulation in the tank is minimal, this would be a realistic representation.

The rotating electrolyser may exhibit a radial velocity profile which is either always positive or which may contain some regions of very small reverse radial flows. Therefore, depending on whether reverse flows are present, the boundary conditions are either of the capillary gap type or of the pump cell type.

With the boundary conditions now specified, by defining the initial condition as zero tracer concentration, the problem formulation is complete.

3.2. *Numerical analysis/program construction*

Transient 2-D modelling of convective diffusion usually requires numerical solution. Owing to the complexities of the pump cell and rotating electrolyser a numerical solution was sought. Simplified models were developed for the capillary gap cell, but even so, an accurate representation over a broad range of parameters requires a numerical solution.

With transient 2-D split boundary value problems the most popular methods are finite differences (FDM) and finite elements (FEM), coupled with a time integration technique. In this case owing to the grid refinement capabilities of the FEM, and the ease with which natural boundary conditions can be implemented, FEM was chosen for this problem.

The spatial terms of the equation were approximated by standard FEM techniques and the time dependence was included by finite difference. The technique was structured so that an implicit solution was obtained. Two approximations in time were employed: the second-order accurate Crank–Nicolson and the first-order forward difference schemes. Although the first method is more accurate, it requires significantly more storage space. Because of this, the first-order method was used, requiring less storage space but more time steps to complete the computation. With the computer used herein, the latter method was the more efficient.

For the system of interest, a flow rate of about $12.5 \times 10^{-6}\ m^3\ s^{-1}$ and a gap width of 0.60 mm, corresponding to a Peclet number on the order of 10^6, were used. Under these conditions the program predicted unphysical concentrations and exhibited severe oscillation. This behaviour is well documented in the literature particularly for the analogous heat transfer problem [8–10]. It is observed that for convection-dominated flows the conventional Galerkin form of the FEM does induce numerical oscillations for anything but an extremely discretized domain. The

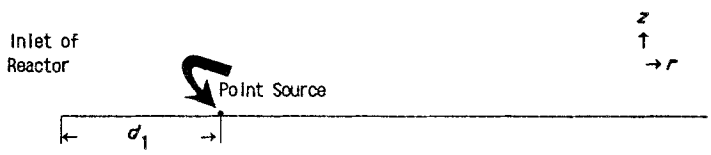

Fig. 2. Inlet boundary conditions for wall tracer.

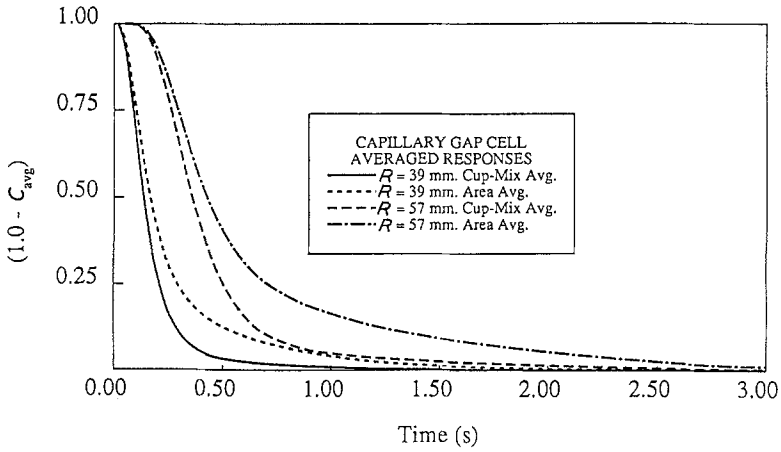

Fig. 3. Capillary gap cell averaged responses. Gap = 0.60 mm and flow rate = 12.5×10^{-6} $m^3 s^{-1}$.

proponents of the Galerkin FEM (GFEM) emphasize that the GFEM is the most accurate of the FEM techniques and that if oscillations result, recourse should be made to discretization [10]. This however may make the problem extremely costly. The other school of thought is that, rather than resorting to excessive discretization, it is preferable to alter the form of the 'arbitrary' trial function (which in the Galerkin form is the basis function). Success, both in accuracy and stability, has been reported by weighing more heavily the 'upstream' or 'upwind' contributions to each element [9, 11, 12] – the upwind side being determined by the orientation of the velocity vector on the side of that element; this approach is known as 'upwinding' or upwind finite elements (UFEM).

From the work of Huyakorn *et al.* [12] and preliminary results using the GFEM it was decided that upwinding techniques should be applied. This was expected to result in computational efficiency without sacrificing too much accuracy [12].

3.3. *Results from the FEM analysis*

Before interpreting the results, two different types of tracer marking and detection should be distinguished. According to Levenspiel *et al.* [13, 14] and Turner [15], only one combination of injection and detection will provide the residence time distribution of the fluid. The other combinations may provide some insight into the problem but do not represent the fluid's history in the vessel. They describe the different injection and detection types as:

Injection A – proportional to local velocity
Injection B – not proportional to velocity
Detection A′ – cup-mix average
Detection B′ – area averaged

which result in four distinct interpretive methods:

Scheme 1 – A–A′
Scheme 2 – A–B′
Scheme 3 – B–A′
Scheme 4 – B–B′

The two averages are defined as:

(1) Cup-mix

$$C_{\text{CMavg}} = \frac{\int_0^a 2\pi r v_r(z)_r C(z, t)_r \, dz}{\int_0^a 2\pi r v_r(z)_r \, dz} \quad (4)$$

(2) Area average

$$C_{\text{Area-avg}} = (1/a) \int_0^a C(z, t)_r \, dz \quad (5)$$

Figure 3 shows the results of Schemes 1 and 2 for the capillary gap cell. The mean residence times calculated from these curves were 0.172 and 0.442 s from Scheme 1 and 0.266 and 0.637 s for Scheme 2. The actual mean residence times at 39 and 57 mm radius are 0.169 and 0.430 s. The first moment of the exit age distribution (or the zeroth moment of the washout function) equals the mean residence time [13] and therefore Scheme 1 is the only tracer analysis which provides the actual representation of the fluid's residence time distribution. Any other mode of injection and detection will not yield the true RTD. If an incorrect RTD was used for reactor calculations considerable errors could result particularly for large Damkohler numbers. Therefore care must be taken in tracer experiment interpretation and design.

It should be emphasized that this is for a closed

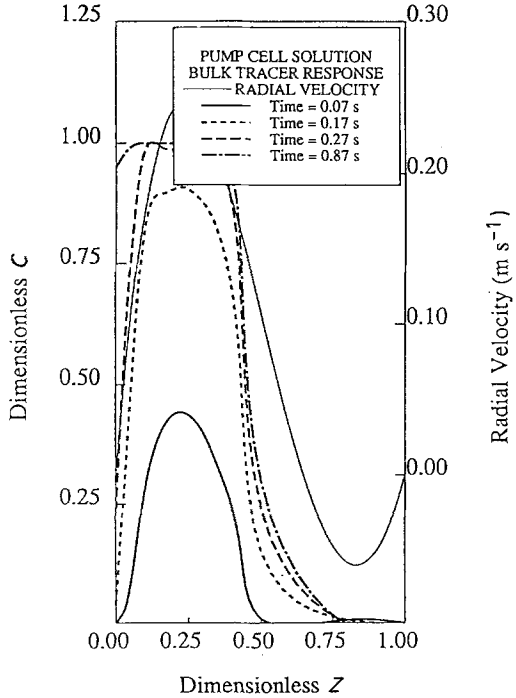

Fig. 4. Pump cell solution at 350 rpm. Bulk tracer response at R = 39 mm. Gap = 0.60 mm and flow rate = 12.5×10^{-6} $m^3 s^{-1}$.

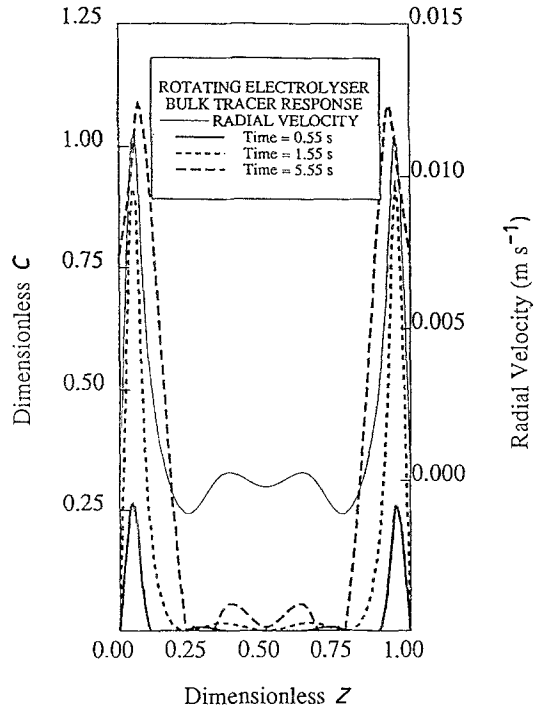

Fig. 5. Rotating electrolyser at α = 11.3. Bulk tracer response at R = 39 mm. Gap = 6.4 mm and flow rate = 3.82 × 10^{-6} m^3 s^{-1}.

system, that is, that each particle enters the system only once; once the particle exits it never re-enters. This is the situation for the capillary gap cell but the pump cell and rotating electrolyser exhibit reverse radial flows over most of the range of their application; this is especially true of the pump cell where the very strong reverse flows are observed. However, since it was assumed that the cells discharge into an infinite CSTR of negligible concentration, the open nature of the two cells is circumvented – they therefore contain two solvent entry zones (R_{in} and R_0) but only one solute injection region. Figures 4 and 5 present the tracer responses for bulk tracer injection. Also plotted are the radial velocity profiles. Figure 4 describes the transport of tracer in the pump cell. Owing to the assumption of the pump cell emptying into an infinite CSTR the lower half of the gap has almost 100% tracer and the upper half is very low in tracer concentration. Sharp concentration gradients exist between the two halves, consistent with the convection-dominated nature of the problem and the boundary conditions used. One other point of interest is that the high reverse flows at larger radius decrease in magnitude at smaller radii. In this case the radial velocities become completely positive at a radius of about 10 mm, and with the significant axial velocities, this pure solvent flow source must be gradually transported out in the radial jet, close to the spinning electrode. This 'dilution' of the tracer jet is exhibited by the region of positive radial flow ($0.50 < z < 0.75$) where only very small changes in concentration are observed over relatively large times – note that below z = 0.50 the concentration is almost 1.0 after 0.87 s. Because of the nature of the pump cell, with its strong reverse flows, washout curves were not generated. Computations made for this cell will be very sensitive to the complete reactor system, including the vessel into which the pump cell empties (and where the reverse flows originate) and actual accumulation in the discharge tank which was not included in the model.

The rotating electrolyser at 350 rpm (corresponding to a Re_θ of 1.0 × 10^5), a flow rate of 12.5 × 10^{-6} m^3 s^{-1} and a gap of 0.60 mm (Taylor number of 1.8) resulted in a profile only slightly different to that of the capillary gap cell; v_r was always positive after the entry region having a slightly flatter appearance than the parabolic profile present in the capillary gap cell. Therefore rather than duplicate the CG response (they would be very close) a much larger Taylor number was used – 11.3. Figure 5 presents the results of this computation also showing the radial velocity profile. In this case the velocity jets very near the electrodes were evident, and as for the convection-dominated nature of this cell, the steep concentration gradients are again indicative. In contrast to the PC, the central portion of the interelectrode gap is very nearly stagnant, and the axial velocities are negligible after the entry length. This is evidenced by the more positive concentrations over the whole region of positive radial velocities: there is much less dilution due to the influx of pure solvent at the exit radius and hence the higher concentrations over the positive velocity zones. (The concentrations greater than 1.0 are due to spline interpolation (in plotting) and were not calculated.) The isolation of the two wall jets from each other can be readily seen and this is the major reason for the separation efficiency of anolyte and catholyte streams observed in previous rotating electrolyser research [16–18].

Wall-generated tracer simulations were then done; these would correspond to an extreme example of injection Scheme B. For this wall injection, the detection was made at the wall in the experiments done by

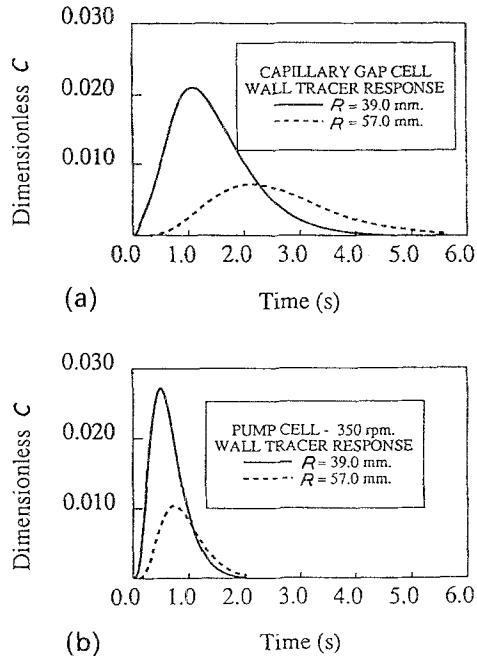

Fig. 6. Wall tracer response at two radii. Gap = 0.60 mm and flow rate = 12.5 × 10^{-6} m^3 s^{-1}. (a) Capillary gap cell; (b) pump cell at 350 rpm.

Fleischmann *et al.* [4]. Figure 6 presents wall tracer responses for the CG and PC, the latter being at 350 rpm. Note that for the same flow rate, the pump cell response is less dispersed. The first moments of these curves at 39 and 57 mm are 1.45 and 2.59 s for the capillary gap cell, 0.65 and 0.91 s for the pump cell and 0.97 and 1.73 s for the REL (response not shown since velocity profile similar to the CG). The first two curves are qualitatively consistent with the results of Fleischmann *et al.* [4], no further comparison being possible owing to a seeming inconsistency in Fig. 3 of that paper [4]. They show no experimental response curve for the pump cell however. Qualitative curves were shown in Ref. [3] and the trend between Figs 6a and 6b (as rotation is included) is confirmed by Fleischmann and Jansson [3]. As rotation is included, their experimental responses become less dispersed.

Calculating the zeroth moment of the wall tracer at successive radii provides an indication of mass exchange between the wall and the bulk of the fluid. A normalized zeroth moment can be defined as

$$M_0 = \frac{\int_0^\infty C_{\text{wall}}(r, \tau)\, d\tau}{\int_0^\infty C_{\text{wall}}(29.5\,\text{mm}, \tau)\, d\tau} \qquad (6)$$

Figure 7a presents a comparison of these normalized zeroth moments for three cells. As mentioned, the REL at these conditions (350 rpm, 0.60 mm gap, 12.5×10^{-6} m^3 s^{-1} flow rate) was similar to the capillary gap cell and hence its zeroth moments, based on wall concentrations, should be close to those of the CG cell. Figure 7a substantiates this. The results of the pump cell were somewhat unexpected however, since the axial velocities are finite and towards the electrode where the tracer was generated. However, in light of the results of Fig. 4, the greater change in zeroth moment in the pump cell would be due to dilution by the incoming solvent.

The same was then done at a lower flow rate 3.82×10^{-6} m^3 s^{-1} at a larger gap (6.4 mm) but was done for only the CG and REL since the 6.4 mm gap was too large to maintain accuracy in the perturbation solution velocities ($\alpha = 3.8$) for the pump cell. This deficiency in velocity prediction has recently been resolved [19]. Figures 7b and 8a present the wall response for the CG and REL. The response for the REL is somewhat sharper than the CG cell for these conditions (figure not included for pump cell under these conditions). An important conclusion is lucidly shown in Fig. 8b. The zeroth moment for the REL at a Taylor number of 11.3 is much higher than in the CG cell at the 57 mm radius, indicative of little mass exchange between the electrode surface and the fluid bulk for the rotating electrolyser.

This provides a conclusive commentary on the separation efficiency of the rotating electrolyser, the Taylor number being the important parameter in separation of the two electrode jets. Since the form of the radial velocities is very insensitive to flow rate for a given Taylor number, the degree of separation can be specified essentially by setting the gap width and rpm for a given Newtonian fluid.

4. Simplified analyses

Two simplified models were then developed for comparison with the rigorous model. Owing to the complex nature of the rotational cells this was done for the capillary gap cell only. The first model developed was based on the assumption that the characteristic diffusion time (t_d) was much larger than the characteristic convection time (t_c). The second model was based upon the t_d/t_c ratio being very small. These will now be

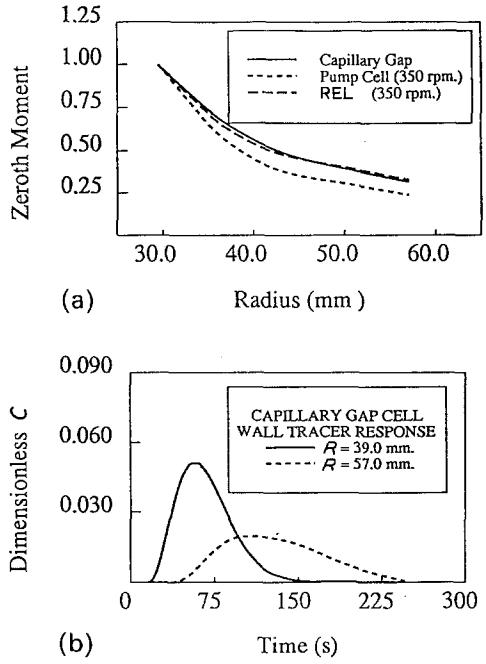

Fig. 7. Wall tracer results. (a) Normalized zeroth moments for wall tracer. Gap = 0.60 mm and flow rate = 12.5×10^{-6} m^3 s^{-1}. (b) Wall tracer response for the CG cell. Gap = 6.40 mm and flow rate = 3.82×10^{-6} m^3 s^{-1}.

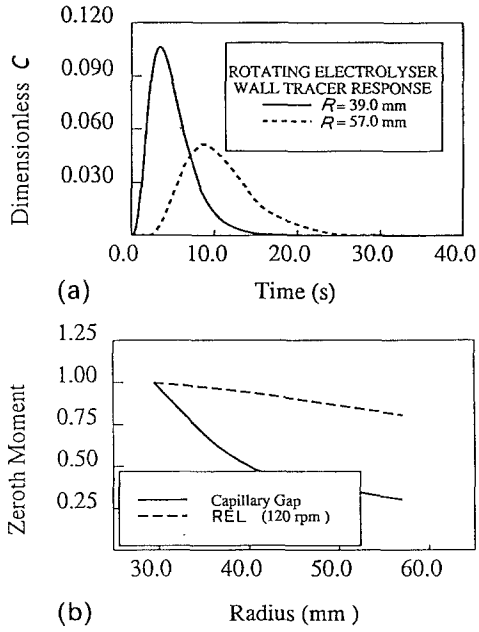

Fig. 8. Wall tracer results. (a) Rotating electrolyser at $\alpha = 11.3$. Response with gap = 6.40 mm and flow rate = 3.83×10^{-6} m^3 s^{-1}. (b) Normalized zeroth moments. Gap = 6.40 mm and flow rate = 3.82×10^{-6} m^3 s^{-1}.

summarized including a comparison with the rigorous model.

4.1. *Pure convection*

For this case, diffusion effects are assumed to be negligible compared to convection. The equation reduces to a first-order partial differential equation.

$$\frac{\partial C}{\partial t} = -v_r \frac{\partial C}{\partial R} \tag{7}$$

where

$$v_r = \frac{v_{RMAX} R_{in}}{R}(1 - z^2) \tag{8}$$

and where $z = Z/a_{1/2}$, where $a_{1/2}$ is the half-gap width.

For a step input of tracer it follows from the pure convection model that the tracer is dispersed into a paraboloid form. To relate the spread of tracer to time and radial distance, an average velocity needs to be defined. This is defined as

$$v_{Ravg\text{-}R} = \frac{2\pi \int_0^R ((v_{RMAX} R_{in})/R)(1 - z^2) R dR}{2\pi \int_0^R R dR} \tag{9}$$

$$= 2v_{RMAX} R_{in}(1 - z^2)/R \tag{10}$$

To relate $v_{RMAX} R_{in}$ to volumetric flow rate Q, the following definition can be used:

$$Q = 4\pi R_{in} a_{1/2} \int_0^1 v_{RMAX}(1 - z^2)\, dz \tag{11}$$

recalling that z is dimensionless but the other variables are dimensional quantities. Integrating, one sees that

$$v_{RMAX} R_{in} = \frac{3Q}{8\pi a_{1/2}} = \frac{3Q}{4\pi a} \tag{12}$$

Therefore

$$v_{Ravg\text{-}R} = \frac{3Q}{2\pi a R}(1 - z^2) \tag{13}$$

and the locus of radial positions defined by this parabolic velocity is then

$$R = \frac{3Q}{2\pi a R} t(1 - z^2) \tag{14}$$

or

$$R^2 = \frac{3Q}{2\pi a} t(1 - z^2) \tag{15}$$

For comparison with the subsequent analysis, where diffusion time is less than convection time, (and where area-averaged quantities are defined), area-averaged concentrations will be computed using Equation 15. After comparing the area averages, the exit age distribution could be generated from this information; although for this step injection of tracer the F curve (cumulative residence time distribution) would be the result and would have to be differentiated to provide the E curve.

Equation 15 can be rearranged to give the axial coordinate, at any radius and time, where tracer is present. By then integrating from $Z = 0$ (centre line) to Z equal to the solution of Equation 15, the area-average concentration (which for the pure convection case is the same as the cup-mix average due to the implicit weighting of the area according to the velocity profile) is obtained. Therefore, solving Equation 15 for Z, as Wen and Fan [1] did for pipe flow

$$Z = \sqrt{\left(1.0 - \frac{2\pi a R^2}{3Qt}\right)} \tag{16}$$

For

$$\frac{2\pi a R^2}{3Qt} \geqslant 1.0; \qquad C_{avg} = 0$$

For

$$\frac{2\pi a R^2}{3Qt} \leqslant 1.0$$

then

$$C_{avg} = \int_0^Z C_0 d\chi \Big/ \int_0^1 d\chi \tag{17}$$

where χ is a 'dummy' integration variable. For the dimensionless concentration defined herein

$$C_{avg} = \sqrt{\left(1.0 - \frac{2\pi a R^2}{3Qt}\right)} \tag{18}$$

the average dimensionless concentrations are thus determined for the pure convection case.

4.2. *Taylor diffusion*

In a classical work, Taylor [20] discusses the dispersion of a solute in very slow pipe flow. He developed a succinct description of the dispersion phenomena reducing the convective diffusion equation to a diffusion equation where the spatial variable was moving at the mean velocity of the flow.

From Equation 2, below reproduced, one has

$$\frac{\partial C}{\partial t} = D\left(\frac{\partial^2 C}{\partial R^2} + \frac{1}{R}\frac{\partial C}{\partial R} + \frac{\partial^2 C}{\partial Z^2}\right) - \left(v_r \frac{\partial C}{\partial R} + v_z \frac{\partial C}{\partial Z}\right) \tag{2}$$

Azimuthal symmetry is assumed as well as constant D. Its assumed that the contribution of diffusion parallel to the mean fluid flow is small compared to the perpendicular diffusion term and that axial velocities are negligible. Equation 2 simplifies to

$$\frac{\partial C}{\partial t} = D\frac{\partial^2 C}{\partial Z^2} - v_r \frac{\partial C}{\partial R} \tag{19}$$

Defining a dimensionless axial coordinate z as $Z/(a/2)$ (in the remainder of the development let $A = a/2$ for brevity), therefore

$$\frac{\partial C}{\partial t} = \frac{D}{A^2}\frac{\partial^2 C}{\partial z^2} - \frac{V_{RMAX} R_{in}}{R}(1 - z^2)\frac{\partial C}{\partial R} \tag{20}$$

Letting $\zeta = R^2$, the equation becomes

$$\frac{\partial C}{\partial t} = \frac{D}{A^2}\frac{\partial^2 C}{\partial z^2} - 2V_{RMAX} R_{in}(1 - z^2)\frac{\partial C}{\partial \zeta} \tag{21}$$

Taylor then defined a coordinate transformation where the longitudinal coordinate is moving at the mean velocity of the fluid. In the radial flow geometry the velocity is decreasing with radius and hence to define a mean velocity a radially averaged areal progression rate is employed. Defining this as $(R^2 - R_{in}^2)/\tau$ (where τ is the mean residence time), the mean progression rate is $Q/2\pi A$. Defining a new coordinate $\xi = \zeta - Qt/(2\pi A)$, including the definition of $V_{RMAX}R_{in}$ (Equation 12) and subtracting this from the convective term in Equation 21 results in

$$\frac{\partial C}{\partial t} = \frac{D}{A^2}\frac{\partial^2 C}{\partial z^2} - \left(\frac{Q}{4\pi A}(1 - 3z^2)\frac{\partial C}{\partial R}\right) \quad (22)$$

Putting into dimensionless form, one obtains

$$\frac{\partial C}{\partial \tau} = \frac{1}{Pe_r}\frac{\partial^2 C}{\partial z^2} - \frac{1}{2}(1 - 3z^2)\frac{\partial C}{\partial r} \quad (23)$$

where $Pe_r = QA/(2\pi R_0^2 D)$ and $r = \xi/R_0^2$.

Taylor defines the characteristic time of diffusion as the time required for the centre-line concentration to deteriorate to $1/e$ of its value or $C_0 e^{-1}$. His determination involved a zero-order Bessel function series. For the capillary gap cell the resulting separated differential equation (in z) was more simple

$$\frac{\partial^2 C}{\partial z^2} + Pe_r\lambda^2 C = 0 \quad (24)$$

The solution of this part of the equation (where $\partial C/\partial R$ was assumed zero for determining t_d) is

$$C = 2\sum_{n=1}^{\infty} \exp\left(-(n\pi)^2\tau/Pe_r\right)\left(B_n \cos\left(\frac{n\pi}{Pe_r^{1/2}}z\right)\right) \quad (25)$$

and where λ_n (eigen values) are defined as

$$\lambda_n = n\pi/Pe_r^{1/2} \quad (26)$$

The term which would decrease the slowest with time would correspond to the smallest eigen value or

$$\lambda_1 = \pi/Pe_r^{1/2} \quad (27)$$

Hence, the time required for the concentration to decay to e^{-1} of its initial value would be

$$\tau_d = \left(\frac{1 + \ln 2}{\pi^2}\right) \quad \text{or} \quad t_d = \frac{(1 + \ln 2)A^2}{\pi^2 D} \quad (28)$$

To be consistent with the initial assumption, this diffusion time (t_d) must be significantly less than the convection time (t_c) defined as (basing t_c on maximum velocity instead of axially averaged velocity)

$$t_c = \frac{2a\pi(R^2 - R_{in}^2)}{3Q} \quad (29)$$

The remainder of Taylor's argument is contingent upon the fact that

$$t_d \ll t_c \quad (30)$$

Since the t_d/t_c relationship changes with radius, the critical radius can be calculated. If the model is applied at radii smaller than the critical radius, the assumptions will not be valid and the model would be expected to fall. Computing R when $t_d = t_c$ one has

$$\frac{(1 + \ln 2)A^2}{\pi^2 D} = \frac{4A\pi(R^2 - R_{in}^2)}{3Q} \quad (31)$$

$$R_c = \sqrt{\left(\frac{3QA(1 + \ln 2)}{4\pi^3 D}\right)} + R_{in}^2$$

From Equation 23, on physical grounds, Taylor argues that any change with time occurs more slowly than the changes due to diffusion and convection; at least $\partial C/\partial t < \partial^2 C/\partial z^2$. This pseudo-steady state assumption should not be too restrictive since the resulting fluxes calculated are later used in an unsteady state mass balance. If Condition 30 is satisfied and $R_{interest} > R_{critical}$ then any perpendicular variation in C disappears very rapidly. This perpendicular variation (i.e. perpendicular to the fluid flow) can then be calculated from the pseudo-steady form of Equation 23, assuming $\partial C/\partial r$ is independent of z since changes in concentration in z occur very rapidly compared to changes with respect to ξ (or r). Therefore

$$\frac{1}{Pe_r}\frac{\partial^2 C}{\partial z^2} = \frac{1}{2}(1 - 3z^2)\frac{\partial C}{\partial r} \quad (32)$$

Involving the boundary conditions that $C(z = 0) = C_1$ and $\partial C(z = 1.0)/\partial z = 0$, one has

$$C(z, r) = C_1 - \frac{Pe}{2}\left(\frac{z^2}{2} + \frac{z^4}{4}\right)\frac{\partial C}{\partial r} \quad (33)$$

To calculate the dimensionless transfer of tracer across the radial perimeter at r, one defines the dimensionless tracer flow as

$$\text{flow} = \int_0^1 \frac{1}{2}(1 - 3z^2)\left(C_1 + \frac{Pe_r}{2}\left(\frac{z^2}{2} - \frac{z^4}{4}\right)\frac{\partial C}{\partial r}\right)dz \quad (33)$$

Upon integrating and substituting the dimensionless quantities one obtains (gmole/time)

$$\text{flow} = -\frac{Q^2 A}{105R_0^2\pi D}\frac{\partial C}{\partial r} \quad (34)$$

Converting back to ζ transformation and doing a mass balance across a differential annular element one obtains

$$\frac{\partial C}{\partial t}2\pi A\, d\zeta = \left(-\frac{Q^2 A}{105\pi D}\frac{\partial C}{\partial \zeta}\right)\Big|_{\zeta} + \left(\frac{Q^2 A}{105\pi D}\frac{\partial C}{\partial \zeta}\right)\Big|_{\zeta + d\zeta} \quad (35)$$

Remembering the definition of the variable ζ with its derivative being $2R\, dR$, after dividing through by $d\zeta$ and taking the limit as $d\zeta$ goes to zero:

$$\frac{\partial C}{\partial t}2\pi A = \frac{Q^2 A}{105\pi D}\frac{\partial^2 C}{\partial \zeta^2} \quad (36)$$

or

$$\frac{\partial C}{\partial t} = \frac{Q^2}{840\pi^2 D R^2}\frac{\partial^2 C}{\partial R^2} \quad (37)$$

By analogy with the classical diffusion equation, the Taylor diffusion coefficient is obtained:

$$\frac{\partial C}{\partial t} = K\frac{\partial^2 C}{\partial R^2} \tag{38}$$

Since diffusion effects are very rapid, the concentration in this equation is representative of the average concentration at any R value. Therefore tracer is dispersed relative to a radius moving at a mean velocity of $Q/(2\pi AR)$ in the same manner as a molecular diffusion process, except that the diffusivity is replaced by the dispersion coefficient K where

$$K = \frac{Q^2}{840\pi^2 DR^2} \text{ or in moving coordinates } (\xi)$$

$$\Gamma = \frac{Q^2}{210D\pi^2}$$

Taylor's expression of K for pipe flow is

$$K = \frac{a^2 u_0^2}{192D} = \frac{Q^2}{192\pi^2 a^2 D} \tag{40}$$

The Taylor diffusivity for the radial geometry is not a function of a owing to the different dependence of t_d and t_c on a in the tube which Taylor described. The approximate solution to Equation 38 for constant K is obtained by Laplace transform of the time derivative and then imposing the boundary conditions on ξ. (It should be noted that the solution is approximate since the boundary conditions include a finite radius and not tracer injection at $R = 0$.) Inversion of the Laplace domain solution, which was

$$C(s, \xi) = (1/s)\exp(-s^{1/2}(\xi/\Gamma^{1/2}))$$

yields (from mathematical tables)

$$C(t, \xi) = 0.50(1.0 - \text{erf}(0.50\xi\Gamma^{-1/2}t^{-1/2})) \quad \xi > 0 \tag{41}$$

By using the transformation for ξ, the average concentration (under the conditions that $t_d \ll t_c$ area-averaged or cup-mix averaged values should provide the same value) can then be computed as a function of time and radius.

4.3. *Results of simplified models*

For a highly convection-dominated flow, the characteristic diffusion time is much larger than the characteristic convection time. The highest flow rate used in this work was $12.5 \times 10^{-6}\,m^3\,s^{-1}$ which corresponded to a Peclet number of about 10^7. For this flow rate $t_d = 15.4\,s$ and $t_c = 0.29\,s$ and therefore the pure convection model should compare more favourably with the numerical solution. This is also reflected by the critical radius being 392 mm while the computations were done at 39 and 57 mm. Figure 9 illustrates this. The small disagreement between the FEM and the convection model is probably due to numerical dispersion in the FEM at small time. The behaviour is well documented in analogous heat transfer problems for upwinding solutions [11, 12]. For the Taylor model, agreement is very poor, as to be expected based on the t_d/t_c ratio and $R_{critical}$ being large. All the inherent assumptions of the Taylor model are grossly in error.

For the next flow rate, $12.5 \times 10^{-8}\,m^3\,s^{-1}$, the comparison is shown in Fig. 10. As expected based on the t_d/t_c ratio (0.54 with $R_c = 4\,mm$), the Taylor predictions are more dispersed than should be the case, although the agreement is much better. The convection model does not provide an adequate representation either. At breakthrough the comparison is quite good but at large time, as tracer is diffusing from the wall layers into the bulk (and transported out), the pure convection model deviates significantly. This result is expected since the tracer can only exit by convection. Since the velocities of the lamenae near the wall are small, the tails of the pure convection model are much longer than would be the case if diffusion effects were present.

The next flow rate, $12.5 \times 10^{-10}\,m^3\,s^{-1}$, corresponded to a t_d/t_c ratio of about 0.005. For this flow rate neither simplified model compared well with the rigorous solution as shown in Fig. 11. The inadequacy of the convection model is readily explained by the lack of diffusion from the wall to the lamenae out. However with the t_d/t_c being about 0.005, the Taylor solution was expected to provide a better match

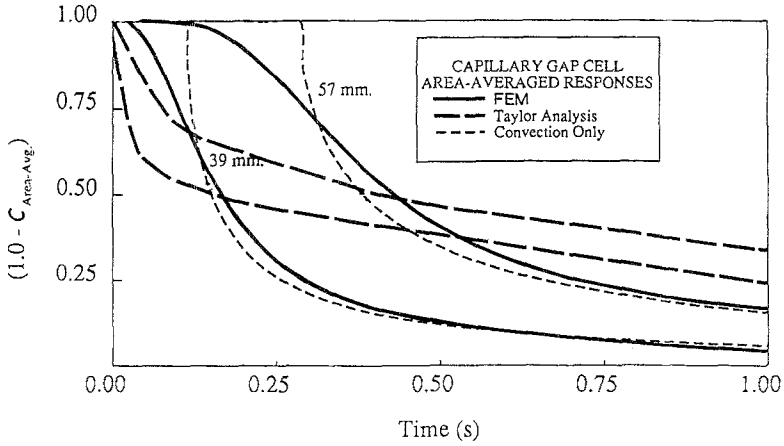

Fig. 9. Capillary gap cell area-averaged responses. Gap = 0.60 mm and flow rate = 12.5×10^{-6} $m^3\,s^{-1}$.

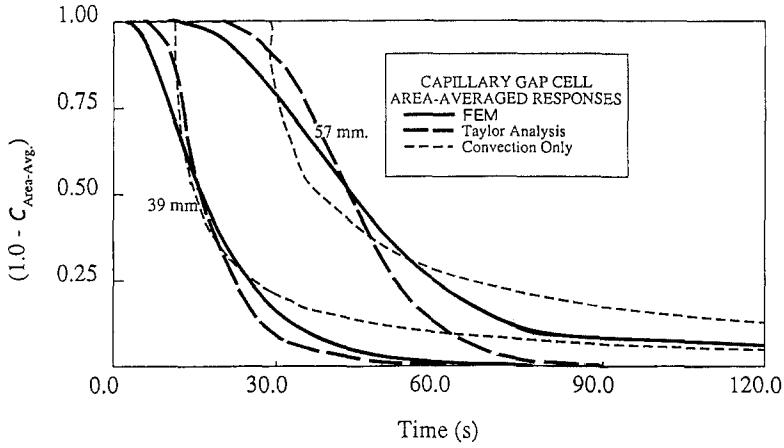

Fig. 10. Capillary gap cell area-averaged responses. Gap = 0.60 mm and flow rate = 12.5×10^{-8} $m^3 s^{-1}$.

($R_{critical}$ = 20.4 mm). The lack of agreement is probably due to having omitted diffusion parallel to the direction of flow. At very low velocities the diffusion parallel to flow will not be negligible. The simple addition of the molecular diffusivity to the Taylor dispersion resulted in excessive dispersion at the lower flow rates and was not investigated further.

In light of this the Taylor diffusivity is not a very versatile tool, although if the radial diffusion terms were included, it could be used for systems where t_d/t_c was less than about 0.01. The pure convection model provided an adequate representation for the averaged tracer response at flows where t_d/t_c was greater than about 100.

It should be mentioned here that a Taylor model was begun for the rotating electrolyser. The methodology followed was the same as for the CG except for the velocity profile. In the CG it was parabolic. In the REL, the least squares technique was used to fit the asymptotic velocities to a polynomial. The applications of the REL will be for high Taylor number and hence the 11.3 Taylor number run was investigated. Using seven points from the velocity predictions (seven points per half gap), a sixth-order polynomial (exact fit) was required to reduce the sum-of-squares error to an acceptable value. When intermediate points were checked very unrealistic profiles were obtained. This was not entirely unexpected owing to the very extreme nature of the velocity profile observed. No further effort was expended to try and gain the Taylor diffusivity model for the REL.

5. Summary of inert tracer modelling

Incorporating the detailed velocity profiles solved for previously [7, 19], inert tracer transport was modelled using the convective diffusion equation. Upwind finite element methods were used to develop a detailed solution to tracer transport in the three radial flow cells under scrutiny: the capillary gap cell, the pump cell and the rotating electrolyser.

It was shown how correct tracer injection and detection must occur in order to infer the correct RTD on the basis of the tracer response.

For the cells where reverse radial flow was present, it was assumed that the system was surrounded by an infinite CSTR, and so the open nature of the rotating cells was not dealt with. To simulate this rigorously, the surrounding equipment would have to be modelled and such was considered beyond the scope of this work.

Bulk- and wall-generated tracers were modelled and interpretations made. Dilution of the wall jet present in the pump cell was shown both for the bulk- and wall-generated tracers. This was seen to be caused by the reverse radial flow of pure solvent with the accompanying finite axial velocities. Comparing the zeroth moment of the wall tracer for the PC with that of the CG it was observed that this dilution decreased the value of this moment considerably below that of the CG cell. In addition it was also shown that the wall response in the PC is much sharper than in the CG, simply owing to the presence of the wall jet in the PC.

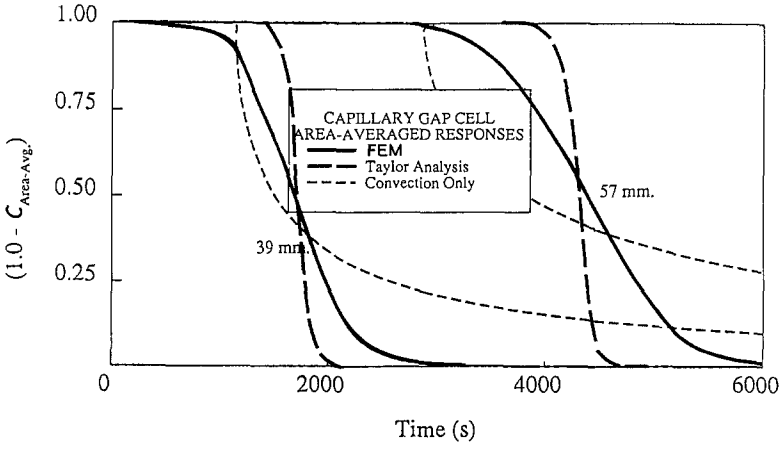

Fig. 11. Capillary gap cell area-averaged responses. Gap = 0.60 mm and flow rate = 12.5×10^{-10} $m^3 s^{-1}$.

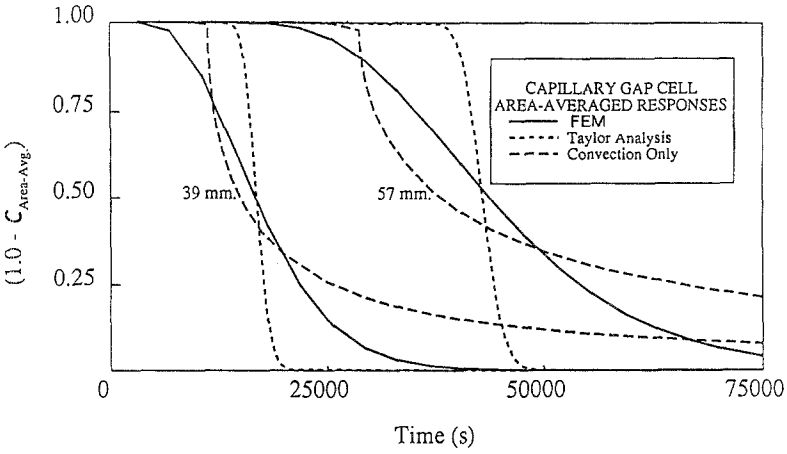

Fig. 12. Capillary gap cell area-averaged responses. Gap = 0.60 mm and flow rate = 12.5×10^{-11} $m^3 s^{-1}$.

It was shown how the REL was an efficient separation device, the degree of separation being a direct function of Taylor number for laminar flow. The REL also exhibited much sharper wall-tracer responses (pulse), again owing to the wall jet being present at higher Taylor numbers.

Simplified models were developed for the capillary gap cell and their limits of application quantified. It was found that for the radial geometry the convection model performed well above a t_d/t_c ratio of 100 and the Taylor diffusion model provides an adequate representation for a t_d/t_c ratio of about 0.10. The same was also attempted for the rotating electrolyser but owing to the extreme form of the radial velocity profile similar simplified solutions proved futile. None were investigated for the pump cell.

Other more accurate simplified solutions could be attempted for the radial geometry, such as using fitting procedures with models like the sum-of-two-zones and the fast- and stagnant-zone models. Such might be entertained at a later time but owing to their empiricism they were not investigated herein.

The impact of these reactors' mixing environments has been investigated using the methoxylation of furan as a model reaction scheme [21]. There it is shown how the mixing influences conversion, selectivity and current efficiency.

Acknowledgement

The authors express their appreciation to Monsanto Corporation for their support of this project over the years 1982–1987. They also thank Hycal Energy Research Laboratories for covering the costs of publication.

References

[1] C. Y. Wen and L. T. Fan, 'Chemical Processing and Engineering', Vol. 3, New York (1975).
[2] T. Z. Fahidy, 'Principles of Electrochemical Reactor Analysis', Elsevier, New York (1985).
[3] M. Fleischmann and R. E. W. Jansson, *J. Appl. Electrochem.* **9** (1979) 427.
[4] M. Fleischmann, J. Ghoroghchian and R. E. W. Jansson, *J. Appl. Electrochem.* **9** (1979) 437.
[5] R. J. Marshall and R. E. W. Jansson, *J. Chem. Technol. Biotechnol.* **30** (1980) 359.
[6] R. E. W. Jansson and R. J. Marshall, *Electrochim. Acta* **27** (1982) 823.
[7] F. B. Thomas, 'Modelling of Laminar Radial-Flow Electrochemical Cells', D.Sc. Thesis, Washington University, St. Louis. MO, USA.
[8] P. M. Gresho, R. L. Lee and R. L. Sani, in 'Recent Advances in Numerical Methods in Fluids', Vol. 1 (edited by C. Taylor and K. Morgan), Pineridge Press, Swansea, UK (1980) pp. 27–79.
[9] J. C. Heinrich, P. S. Huyakorn, O. C. Zienkiewicz and A. R. Mitchell, *Num. Meth. Eng.* **11** (1977) 131.
[10] P. M. Gresho and R. L. Sani, Finite Element Methods in Convection Dominated Flows, ASME, AMD (1979) pp. 37–49.
[11] P. S. Huyakorn, *Appl. Math. Model.* **1** (1977) 187.
[12] P. S. Huyakorn, *Appl. Math. Model.* **3** (1979) 7.
[13] O. Levelspiel and J. C. R. Turner, *Chem. Eng. Sci.* **25** (1970) 1605.
[14] O. Levelspiel, B. W. Lai and C. Y. Chetilynne, *Chem. Eng. Sci.* **25** (1970) 1611.
[15] J. C. R. Turner, *Chem. Eng. Sci.* **26** (1971) 549.
[16] R. E. W. Jansson, *Electrochim. Acta* **23** (1978) 1345.
[17] R. E. W. Jansson and R. J. Marshall, *J. Appl. Electrochem.* **8** (1978) 287.
[18] A. B. Ferreira and R. E. W. Jansson, *Trans. Inst. Chem. Eng.* **57** (1979) 262.
[19] F. B. Thomas, P. A. Ramachandran, M. P. Dudukovic and R. E. W. Jansson, *J. Appl. Electrochem.* **18** (1988) 768.
[20] G. Taylor, *Proc. R. Soc. A* **219** (1953) 186.
[21] F. B. Thomas, P. A. Ramachandran, M. P. Dudukovic and R. E. W. Jansson, *J. Appl. Electrochem.* **19** (1989) 856.